Angularly-dependent finite difference Vlasov equations

Brody Bassett

April 27, 2016

1 Introduction

The Vlasov equation is used to solve for the time-dependent plasma particle density in a medium where the primary forces between particles is Coulomb interaction. In practice, this means that the Vlasov equation is used to simulate hot particles with low density. If the particles become too cold, they begin experiencing atomic physics, which are less collective than long-range particle interactions.

The normalized Vlasov equation (with q_s/m_s absorbed into the other terms) is

$$\frac{\partial}{\partial t} f_s + \boldsymbol{v} \cdot \nabla_x f_s + (\boldsymbol{E} + \boldsymbol{v} \times \boldsymbol{B}) \cdot \nabla_v f_s = 0, \quad (1)$$

where ∇_x and ∇_v represent the gradients in space and velocity. After solving for the particle density f_s, the charge density and current can be calculated as

$$\rho = \sum_s \rho_s = \sum_s q_s \int_{-\infty}^{\infty} f_s(\boldsymbol{x}, \boldsymbol{v}, t)\, d\boldsymbol{v}^3, \quad (2a)$$

$$\boldsymbol{j} = \sum_s \boldsymbol{j}_s = \sum_s q_s \int_{-\infty}^{\infty} \boldsymbol{v} f_s(\boldsymbol{x}, \boldsymbol{v}, t)\, d\boldsymbol{v}^3. \quad (2b)$$

These equations are solved in tandem with Maxwell's equations,

$$\nabla_x \cdot \boldsymbol{E} = \frac{\rho}{\epsilon_0}, \quad (3a)$$

$$\nabla_x \times \boldsymbol{B} - \frac{1}{c^2}\frac{\partial \boldsymbol{E}}{\partial t} = \mu_0 \boldsymbol{j}, \quad (3b)$$

$$\nabla_x \times \boldsymbol{E} + \frac{\partial \boldsymbol{B}}{\partial t} = 0, \quad (3c)$$

$$\nabla_x \cdot \boldsymbol{B} = 0. \quad (3d)$$

Of these, only the first (Gauss's law) will be used in this simulation to calculate the electric field from the charge density.

The Vlasov equation has been inspected asymptotically in a spherical coordinate system with similar variables to the ones used here [1]. Various solution methods have been used to solve the Vlasov equation, including discontinuous Galerkin methods [2], finite volume methods [3] and spherical harmonics expansions [4]. Methods based on the method of characteristics have also been explored [5]. The Vlasov equations have the same numerical limit as the particle-in-cell methods. While more expensive to solve, the Vlasov equations don't suffer from the same numerical noise as the particle-in-cell methods [6].

2 Numerical model

2.1 Three-dimensional transformation

The following three-dimensional model is written using three dimensions in space, two dimensions in angle and one dimension in velocity. First, write the Vlasov equation in conservative form:

$$\frac{\partial}{\partial t} f_s + \nabla_x \cdot \boldsymbol{v} f_s + \nabla_v \cdot (\boldsymbol{E} + \boldsymbol{v} \times \boldsymbol{B}) f_s = 0. \quad (4)$$

This transformation from Eq. 1 is valid because $(\boldsymbol{v} \times \boldsymbol{B})_i$ does not depend on v_i. Use the variable transformation of Dogbe [7] from $\boldsymbol{v} \to v, \boldsymbol{\Omega}$ with

$$v = |\boldsymbol{v}| = \sqrt{v_x^2 + v_y^2 + v_z^2}, \quad (5a)$$

$$\boldsymbol{\Omega} = \frac{1}{v}\{v_x, v_y, v_z\}, \quad (5b)$$

to get (after much algebra) the conservative form of the velocity gradient in terms of the scalar velocity derivative and the angular gradient,

$$\nabla_v f = \boldsymbol{\Omega}\frac{\partial f}{\partial v} + \frac{1}{v}\nabla_\Omega f - \frac{1}{v}(\nabla_\Omega \cdot \boldsymbol{\Omega})\boldsymbol{\Omega} f. \quad (6)$$

Converting the other operators using the same transformations, the equations become

$$\frac{\partial}{\partial t} f_s + v\nabla_x \cdot \boldsymbol{\Omega} f_s + \nabla_v \cdot (\boldsymbol{E} + v\boldsymbol{\Omega} \times \boldsymbol{B}) f_s = 0, \quad (7)$$

with ∇_v from Eq. 6.

2.2 One-dimensional transformation

The following transformation is written using one spatial dimension, one angular dimension and one velocity dimension. First, restrict the original Vlasov equation (Eq. 4) to one spatial and two velocity dimensions, with $\boldsymbol{B} = B_z\hat{\boldsymbol{z}}$, to get

$$\frac{\partial}{\partial t}f_s + \frac{\partial}{\partial x}v_x f_s + \frac{\partial}{\partial v_x}\left(E_x + v_y B_z\right) + \frac{\partial}{\partial v_y}\left(E_y - v_x B_z\right) f_s = 0. \quad (8)$$

Using the variables

$$v = \sqrt{v_x^2 + v_y^2}, \quad (9a)$$

$$\gamma = \arctan\frac{v_y}{v_x}, \quad (9b)$$

the equation can be transformed using a standard cylindrical geometry transformation,

$$\nabla_v f = \frac{\partial f}{\partial v}\left(\cos\gamma\hat{\boldsymbol{x}} + \sin\gamma\hat{\boldsymbol{y}}\right) + \frac{1}{v}\frac{\partial f}{\partial\gamma}\left(-\sin\gamma\hat{\boldsymbol{x}} + \cos\gamma\hat{\boldsymbol{y}}\right), \quad (10)$$

to get

$$\frac{\partial}{\partial t}f_s + v\cos\gamma\frac{\partial}{\partial x}f_s + \left[E_x\cos\gamma + E_y\sin\gamma\right]\frac{\partial}{\partial v}f_s + \frac{1}{v}\frac{\partial}{\partial\gamma}\left[-E_x\sin\gamma + E_y\cos\gamma - vB_z\right]f_s = 0 \quad (11)$$

for the bounds

$$0 \le x \le X, \quad (12a)$$

$$0 \le v < \infty, \quad (12b)$$

$$0 \le \gamma \le 2\pi, \quad (12c)$$

$$0 \le t < \infty. \quad (12d)$$

As expected, the magnetic field term appears only in the angular derivative. This means that the magnetic field cannot directly change the particle velocity. The boundary conditions are

$$f_s\left(0, v, \gamma, t\right) = f\left(X, v, \gamma, t\right), \quad (13a)$$

$$\lim_{\epsilon\to 0^+} f_s\left(x, \epsilon, \gamma, t\right) = \lim_{\epsilon\to 0^-} f_s\left(x, \epsilon, \gamma + \pi, t\right), \quad (13b)$$

$$\lim_{v\to\infty}\frac{\partial}{\partial v}f_s\left(x, v, \gamma, t\right) = 0, \quad (13c)$$

$$f_s\left(x, v, 0, t\right) = f_s\left(x, v, 2\pi, t\right), \quad (13d)$$

$$f_s\left(x, v, \gamma, 0\right) = g\left(x, v, \gamma\right), \quad (13e)$$

These correspond to periodic boundaries for the x and γ dimensions, reflective for the upper velocity bound, and an initial condition on the time. By definition, the velocity cannot go below zero. Thus, when the velocity would go below zero, the angle instead reverses direction.

2.3 Finite difference equations

The derivatives will be discretized using a central finite difference scheme,

$$\frac{\partial}{\partial x}f = \frac{f_{i+1} - f_{i-1}}{2\Delta x}, \quad (14a)$$

$$\frac{\partial}{\partial v}f = \frac{f_{g+1} - f_{g-1}}{2\Delta v}, \quad (14b)$$

$$\frac{\partial}{\partial\gamma}f = \frac{f_{n+1} - f_{n-1}}{2\Delta\gamma}, \quad (14c)$$

with the indices i, g, n, ℓ representing, respectively, the spatial, velocity, angular and temporal time points. The species index, s, will be suppressed. The equation

$$\frac{\partial}{\partial t}f_{i,g,n}\left(t\right) + h_{i,g,n}\left(t\right) = 0, \quad (15)$$

will be discretized using a finite volume (or Crank-Nicolson) scheme. Apply the operation $\frac{1}{\Delta t}\int_{t_\ell}^{t_{\ell+1}}\left(\cdot\right)dt$ to this equation and interpolate linearly between the endpoints to get

$$\frac{2f_{i,g,n}^{(\ell+1)}}{\Delta t} + h_{i,g,n}^{(\ell+1)} = \frac{2f_{i,g,n}^{(\ell)}}{\Delta t} - h_{i,g,n}^{(\ell)}, \quad (16a)$$

with

$$h_{i,g,n} = \frac{\xi_{g,n}\left(f_{i+1,g,n} - f_{i-1,g,n}\right)}{2\Delta x_i} + \frac{\eta_{i,n}\left(f_{i,g+1,n} - f_{i,g-1,n}\right)}{2\Delta v_g}$$

$$+ \frac{\zeta_{i,g,n+1} f_{i,g,n+1} - \zeta_{i,g,n-1} f_{i,g,n-1}}{2\Delta\gamma_n} \quad (16b)$$

and

$$\xi_{g,n} = v_g \cos\gamma_n, \quad (16c)$$

$$\eta_{i,n} = \frac{q_s}{m_s} \left[E_{x,i} \cos\gamma_n + E_{y,n} \sin\gamma_g \right], \quad (16d)$$

$$\zeta_{i,g,n} = \frac{q_s}{m_s} \frac{1}{v_g} \left[-E_{x,i} \sin\gamma_n + E_{y,i} \cos\gamma_n - v_g B_{z,i} \right]. \quad (16e)$$

The boundary conditions on these equations will be

$$f_{i,g,n} = f_{I+1-i,g,n}, \qquad i = 1, I, \quad (16f)$$

$$f_{i,g-1,n} = f_{i,g,n+N/2}, \qquad g = 1, \quad (16g)$$

$$f_{i,g+1,n} = f_{i,g-1,n}, \qquad g = G, \quad (16h)$$

$$f_{i,j,k} = f_{i,j,K+1-k}, \qquad k = 1, K. \quad (16i)$$

With the equations discretized thus from the conservative equations, a sum over i, g, n of Eq. 16a will give an important result,

$$\sum_{i,g,n} f_{i,g,n}^{(\ell+1)} = \sum_{i,g,n} f_{i,g,n}^{(\ell)},$$

which means that the total number of particles in the simulation is not changing in time.

The density and mean density can be calculated using the trapezoidal rule to get

$$F_{i,g} = \sum_{n=1}^{N} (\gamma_{n+1} - \gamma_n) \left(\frac{f_{i,g,n} + f_{i,g,n+1}}{2} \right), \quad (17a)$$

$$\rho_i = q \sum_{g=1}^{G-1} (v_{g+1} - v_g) \left(\frac{v_g F_{i,g} + v_{g+1} F_{i,g+1}}{2} \right). \quad (17b)$$

Following this, the deviation from the average perturbation $\delta\rho_i$ is calculated. Then the electric field is calculated from the finite volume approximation to the equation

$$\frac{\partial}{\partial x} \delta E = \delta\rho, \quad (18)$$

which is found by performing the operation $\int_i^{i+1} (\cdot)\, dx$ and interpolating linearly between the endpoints (as with the time discretization of Eq. 16a) to get

$$\frac{\delta E_{i+1} - \delta E_i}{\Delta x} = \frac{\delta\rho_{i+1} + \delta\rho_i}{2}. \quad (19)$$

As the deviation from the average electric field δE_i is desired, two simple options for boundary conditions exist. First, the zero-mean condition,

$$\sum_i \delta E_i = 0, \quad (20)$$

can be used but isn't ideal computationally when used in a sparse matrix algorithm. Instead, a simple Dirichlet boundary condition of zero at any point can be used, i.e.

$$\delta E_1 = 0, \quad (21)$$

followed by an additive normalization to satisfy the zero-mean condition above (as occurred with the charge density).

3 Results

3.1 Code

The code used to generate the results is based on the finite difference equations listed in Sec. 2.3. The equations for the density f_s and charge density $\delta\rho$ in Eqs. 16 and 19 are solved using Sandia National Laboratory's Trilinos package [8]. The sparse matrix storage is accomplished using the class Epetra. The systems of equations are solved using the class AztecOO with a Jacobi preconditioner and a GMRES solver. The parallelism in the code is implemented with MPI for data transfer and natively within the Trilinos classes. The source code is available at `https://github.com/brbass/phoenix`.

3.2 Test parameters

The tests were initialized using a monoenergetic density of

$$f(x, v_0, \gamma, t) = f_0 + \delta f_0 \left[\sin(2\pi k_x x) + \sin(2\pi k_\gamma \gamma) \right], \quad (22)$$

with a constant magnetic field of

$$B_z(x) = B_0.$$

	Stand. 1	Stand. 2	Upper	Rot.
Num x	100	100	100	10
Δx	0.01	0.01	0.01	1.0
Num v	5	5	5	5
Δv	0.1	0.1	0.1	0.1
Num γ	16	2	16	64
Num t	10001	10001	10001	10001
Δt	0.001	0.001	0.001	0.001
B_0	0.0	0.0	10.0	1.0
f_0	100.0	100.0	100.0	1.0
δf_0	1.0	1.0	1.0	1.0
v_0	0.25	0.25	0.25	0.25
k_x	1.0	1.0	1.0	0.0
k_γ	0.0	0.0	0.0	$1/2\pi$

Table 1

The parameters used for the tests can be seen in Table 1. The four tests are

- Standing 1: Standing wave with many directions,
- Standing 2: Standing wave with two directions,
- Upper: Upper hybrid wave with spatial perturbation, and
- Rotation: Rotation of an angular perturbation.

3.3 Standing wave

The standing wave is a simple sinusoidal wave in the x direction that propagates in time. The standing wave with 16 directions has a lower wavenumber than the standing wave with 2 directions. The standing wave with 2 directions effectively simulates particles moving in the angles $\gamma = 0, \pi$, which causes the angular derivative to go away and the velocity derivative to lack dependence on γ. Because of this, the standing wave has a wavenumber of 1.0, as would be seen in a particle-in-cell code for particles with no initial velocity. The standing wave with 16 directions has a lower wavenumber of about 0.8. The velocity of the particles in this case is not all directed in the $\hat{\boldsymbol{x}}$ direction, so the velocity at which the waves travel will be less than in the case with two directions.

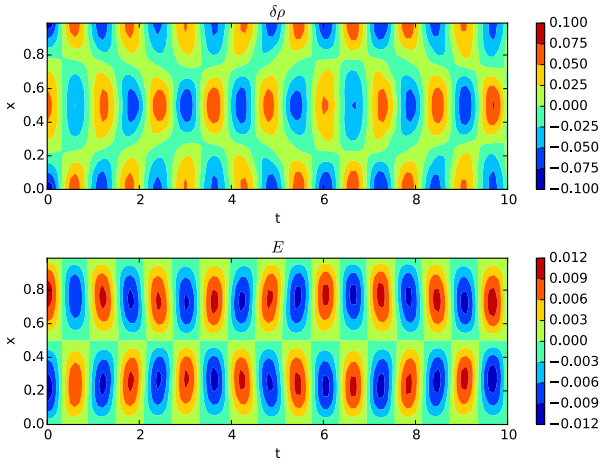

(a) Standing 1, 16 angles

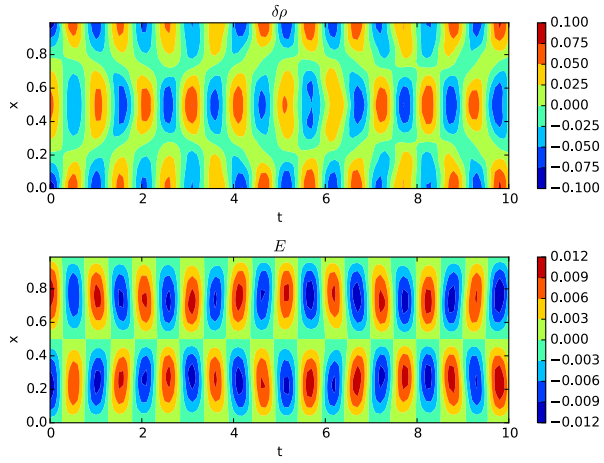

(b) Standing 2, 2 angles

Figure 1: Charge density and electric field

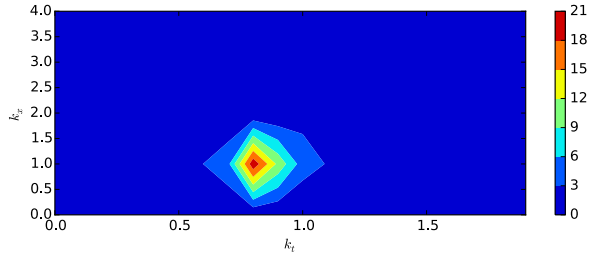

(a) Standing 1, 16 angles

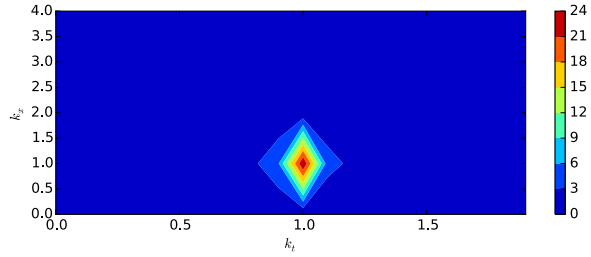

(b) Standing 2, 2 angles

Figure 2: Fourier transform of electric field

Figs. 1a and 1b show the electric fields and charge densities for these two cases. Figs. 2a and 2b show the Fourier transforms of the electric field.

3.4 Upper hybrid wave

In the upper hybrid wave, the oscillation of the particles around the magnetic field lines cancels out the oscillations and causes the waves to rebound.

Fig. 3 shows the charge density and electric field for the upper hybrid wave.

3.5 Rotation

With a monoenergetic initial density with no spatial dependence and no external electric field, Eq. 11 simplifies to

$$\frac{\partial}{\partial t} f_s = B_0 \frac{\partial}{\partial \gamma} f_s, \tag{23}$$

which for an initial density of

$$f\left(x, v, \gamma, 0\right) = f_0 + \delta f_0 \sin\left(\gamma\right) \tag{24}$$

has the solution

$$f\left(x, v, \gamma, t\right) = f_0 + \delta f_0 \sin\left(\gamma + B_0 t\right), \tag{25}$$

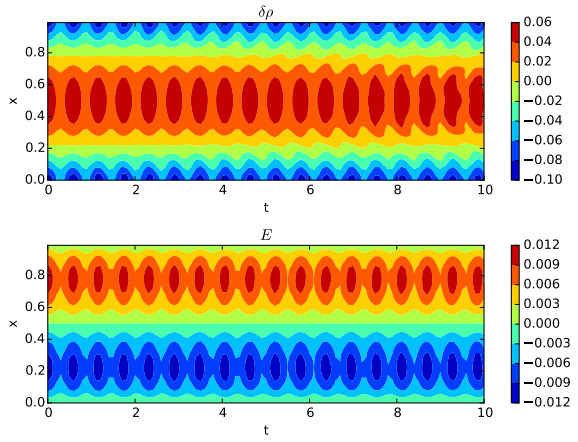

Figure 3: Upper hybrid, Charge density and electric field

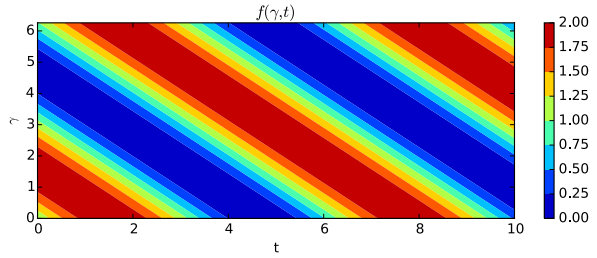

Figure 4: Rotation, Angular dependence of solution

which has a period of

$$\tau = \frac{2\pi}{B_0}. \tag{26}$$

The finite difference approximation depends on smoothness to be an accurate approximation to the derivative of a function. As such, the initial directional dependence was chosen to be a known function with known derivatives. Fig. 4 shows the angular dependence of the time-dependent solution. The wave clearly rotates with the expected frequency.

4 Conclusion

The Vlasov code exhibits many of the same behaviors seen in particle-in-cell methods. The waves have the expected wavenumbers and are conservative as expected.

References

[1] ES Cheb-Terrab and AG Elfimov. The solution of vlasov's equation for complicated plasma geometry. i. spherical type. *Computer physics communications*, 85(2):251–266, 1995.

[2] Blanca Ayuso de Dios, José A Carrillo, and Chi-Wang Shu. Discontinuous galerkin methods for the multi-dimensional vlasov–poisson problem. *Mathematical Models and Methods in Applied Sciences*, 22(12):1250042, 2012.

[3] Francis Filbet, Eric Sonnendrücker, and Pierre Bertrand. Conservative numerical schemes for the vlasov equation. *Journal of Computational Physics*, 172(1):166–187, 2001.

[4] Karl Rupp. *Numerical solution of the Boltzmann transport equation using spherical harmonics expansions*. na, 2009.

[5] Nicolas Crouseilles, Thomas Respaud, and Eric Sonnendrücker. A forward semi-lagrangian method for the numerical solution of the vlasov equation. *Computer Physics Communications*, 180(10):1730–1745, 2009.

[6] Nina V Elkina and Jörg Büchner. A new conservative unsplit method for the solution of the vlasov equation. *Journal of Computational Physics*, 213(2):862–875, 2006.

[7] Christian Dogbe. Spherical harmonics expansion of the vlasov-poisson initial bounary value problem. *arXiv preprint math/0511103*, 2005.

[8] Michael A Heroux, Roscoe A Bartlett, Vicki E Howle, Robert J Hoekstra, Jonathan J Hu, Tamara G Kolda, Richard B Lehoucq, Kevin R Long, Roger P Pawlowski, Eric T Phipps, et al. An overview of the trilinos project. *ACM Transactions on Mathematical Software (TOMS)*, 31(3):397–423, 2005.